Journal of the Meteorological Society of Japan

EARLY ONLINE RELEASE

The DOI for this manuscript is
DOI:10.2151/jmsj.2023-001
J-STAGE Advance published date: October 7th, 2022
The final manuscript after publication will replace the preliminary version at the above DOI once it is available.

What Percentage of Silk-Road Pattern Trigger Pacific–Japan Pattern through Rossby Wave Breaking?

Kazuto TAKEMURA[1]

Climate Prediction Division, Japan Meteorological Agency, Tokyo, Japan

and

Hitoshi MUKOUGAWA

Graduate School of Science, Kyoto University, Kyoto, Japan

----

1) Corresponding author: Kazuto Takemura, Japan Meteorological Agency, 3-6-9 Toranomon, Minato City, Tokyo 105-8431, Japan.

Email: k-takemura@met.kishou.go.jp

Tel: +81-75-xxxx-xxxx

Fax: +81-75-xxxx-xxxx

Abstract

In this study, we investigate the rate at which the Silk-Road pattern (SRP) with Rossby wave breaking (RWB) near the Asian jet exit causes the Pacific–Japan (PJ) pattern in boreal summer. Here, the SRP case is detected using the two principal components of upper-tropospheric meridional winds over Eurasia and characterized by the presence of an upper-level anticyclonic anomaly over the Yellow Sea or near Japan. They are further classified into cases with and without RWBs.

In the SRP case with RWB, the upper-level anticyclonic anomaly near the Asian jet exit has more extended shape in the zonal direction and larger amplitude than in the case without RWB. In the composite, a wave train associated with the SRP appears over Eurasia, which is accompanied by the RWB near the Asian jet exit. The occurrence of RWB is associated with strong deceleration and diffluence in the basic state there. The RWB promotes enhanced convection on its southern side due to the intrusion of upper-level high potential vorticity toward the southwest, resulting in the formation of the PJ pattern. The excited PJ pattern in the composite has a dipole structure with cyclonic anomalies to the south and anticyclonic anomalies to the north. Approximately 60–70% of the SRP case with RWB is accompanied by the PJ patterns.

On the other hand, in the case of the SRP without RWB, the composite represents a wave train structure over Eurasia but indicates neither enhanced convection south of the RWB nor PJ patterns. Approximately 40–50% of the SRP case without RWBs is accompanied by

the PJ patterns. Hence, the presence of RWBs increases the percentage of the formation of positive PJ patterns by a factor of 1.2 to 1.7, indicating that the RWB plays an important role in the excitation of PJ patterns.

Keywords teleconnection; wave breaking; subtropical jet; convective rain

1. Introduction

The Silk Road pattern (SRP) is the dominant teleconnection pattern along the Asian jet in boreal summer (Lu et al. 2002, Enomoto et al. 2003). The SRP can be extracted as the dominant EOF mode of upper tropospheric meridional wind anomalies over mid-latitude Eurasia (e.g., Kosaka et al. 2009, Song et al. 2013, Hong et al. 2018, Zhou et al. 2019). The SRP is also often accompanied by an anticyclone with an equivalent barotropic structure in the troposphere, namely the Bonin high (Enomoto 2004), and the anticyclone can produce unprecedented heat waves around Japan (e.g., Enomoto et al. 2009). The amplified Bonin high is closely associated with the generation of Rossby wave breaking (RWB) (Postel and Hitchman 1999, 2001, Abatzoglou and Magnusdottir 2006), which causes the equatorward penetration of upper-level high potential vorticity (PV) into the subtropical western North Pacific (WNP). The equatorward intrusion of high PV can, in some cases, trigger enhanced convection (Takemura et al. 2017) and the development of tropical cyclones (Takemura and Mukougawa 2021b).

The Pacific–Japan (PJ) pattern is also one of the dominant teleconnection patterns of East Asia, characterized by a meridional dipole structure consisting of circulation anomalies near the Philippines and circulation anomalies with opposite signs near Japan in the lower troposphere (Nitta 1987, Kosaka and Nakamura 2006). Hereafter, the phase with cyclonic (anticyclonic) circulation anomalies near the Philippines and anticyclonic (cyclonic) circulation anomalies near Japan is referred to as the positive (negative) PJ pattern.

Enhanced convection over the subtropical WNP is closely associated with a positive PJ pattern (Wakabayashi and Kawamura 2004), corresponding to the extension of the North Pacific subtropical high over mainland Japan (e.g., Lu and Dong 2001).

From a lag composite analysis of the RWB near Japan occurred in past decades, Takemura and Mukougawa (2020a) showed that there is a dynamical process in which Rossby wave propagation along the Asian jet, including the SRP, promotes the formation of a positive PJ pattern through the RWB near Japan. They emphasized that RWBs play a crucial role in the above dynamical process as follows. The RWB causes high PV intrusion into the subtropical WNP, where dynamically induced upwelling anomalies enhance convection, and consequently contributes to the formation of a positive PJ pattern. The lag composites revealed the SRP, RWB, and the positive PJ pattern peaking in sequence over a period of about one week. This result indicates a close relationship between the SRP with RWB and the positive PJ pattern. The maintenance mechanism of RWBs and positive PJ patterns by the dynamical interaction between them was also statistically elucidated by Takemura and Mukougawa (2020b). Whether or not the SRP accompanies the RWB near the Asian jet exit region is partly related to the deceleration and diffluence of the Asian jet in the region (Takemura et al. 2021).

Takemura and Mukougawa (2022) evaluated the proportion of PJ patterns with RWB by classifying positive PJ patterns into those with and without RWB. They showed that PJ patterns without RWBs are significantly associated with tropical SST anomalies such as El

Niño southern oscillation (ENSO), the basin-wide SST warming in the Indian Ocean (e.g., Xie et al. 2009, 2016), and Pacific meridional mode of SST (Chiang and Vimont 2004, Takaya 2019). They also showed that the PJ pattern without RWB is related to convective anomalies associated with the boreal summer intraseasonal oscillation (BSISO; Kikuchi et al. 2012, Lee et al. 2013, Kikuchi 2021, Seiki et al. 2021) and the bi-week oscillation (Zhu et al. 2020), indicating the importance of the tropical environment for PJ pattern excitation.

On the other hand, although Takemura and Mukougawa (2020a) showed from their composite analyses that SRP can excite PJ pattern through RWBs, a quantitative evaluation of the ability of SRP to excite PJ patterns has not yet been performed. Hence, in this study, we will evaluate the percentage of SRP cases where RWBs around Japan cause positive PJ patterns, and examine the difference in the probability of PJ pattern formation with and without RWBs. This approach is important for re-examining and highlighting the role of RWB in the connectivity between SRP and PJ patterns (Takemura and Mukougawa 2020a). To accomplish this task, we follow the method adopted by Takemura and Mukougawa (2022) to perform lag composite analysis of the SRP case with and without RWBs.

2. Data and methods

To analyze atmospheric circulation, we used daily mean data set of the Japanese 55-year reanalysis (JRA-55) from June to September (JJAS) during the 61-year period from 1958 to 2018, with the horizontal resolution of 1.25° and 37 pressure levels from 1000 to 1 hPa

(Kobayashi et al. 2015). Here, anomaly is defined as the difference from the climatology. The climatology is obtained by a 60-day low-pass (Lanczos; Duchon 1979) filtered daily mean for the 30-year period from 1981 to 2010. To extract the low-frequency components, including quasi-stationary Rossby waves, a five-day running average was applied to the daily data. In order to smooth the relative vorticity field horizontally, a triangular truncation (T24) retaining total wavenumber 24 is used to eliminate disturbances with horizontal scales smaller than the synoptic eddies. The statistical significance of the composited anomalies was assessed by two-tailed Student's *t*-test. The variable *t* is defined as $t = \overline{x'}/\sqrt{\sigma^2/(N-1)}$, where $\overline{x'}$ is the composited anomalies, σ is the standard deviation, N is the number of cases. The variable t obeys a Student's t-distribution with $N-1$ degrees of freedom.

The propagation of Rossby wave packets was analyzed using the wave activity flux (WAF) defined by Takaya and Nakamura (2001). The horizontal WAF is defined as follows:

$$\boldsymbol{W} = \frac{1}{2|\boldsymbol{U}|}\begin{pmatrix} \bar{u}(\psi_x'^2 - \psi'\psi_{xx}') + \bar{v}(\psi_x'\psi_y' - \psi'\psi_{xy}') \\ \bar{u}\left(\psi_x'\psi_y' - \psi'\psi_{xy}'\right) + \bar{v}(\psi_y'^2 - \psi'\psi_{yy}') \end{pmatrix}, \qquad (1)$$

where u is the zonal wind, v is the meridional wind, $\boldsymbol{U}$ is the climatological horizontal wind vector, and ψ is the geostrophic stream function at a reference latitude of $\phi_0 = 40^{\circ}\mathrm{N}$. The reference latitude was selected based on the central latitude of the climatological Asian jet in midsummer (green shading in Fig. 1). The overbars (primes) denote the climatology (anomaly from the climatology). The subscripts x and y denote the partial derivatives with respect to longitude and latitude, respectively.

The detection of SRP cases was performed using EOF modes of monthly mean 200-hPa meridional wind anomalies in the region of [20–60ºN, 30–130ºE] (blue box in Fig. 1 labeled by "SRP") for 61 years from 1958 to 2018, according to Kosaka et al. (2009). We used the averaged field over the two months of July and August to conduct the EOF analysis because these months correspond to the midsummer after the rainy season near Japan. Note that the EOF pattern obtained from the monthly mean meridional wind anomalies is almost the same as the pattern obtained from five-day running mean ones (not shown). The SRP index was defined based on scores PC1 and PC2 ("PC" stands for principal component) of five-day running mean meridional wind anomalies projected on the obtained first and second EOF patterns as follows. Here the EOF pattern is normalized by the standard deviation in July and August during the 61 years. To focus on the anticyclonic anomaly associated with RWB near the Asian jet exit, positive PC1 and negative PC2 scores were adopted as SRP indicators. The results of regressing 200-hPa vorticity anomalies on positive PC1 and negative PC2 scores (Fig. 2) show that anticyclonic anomalies exist over the Yellow Sea and around Japan (red boxes in Fig. 2), respectively. Here, the SRP case is extracted when the absolute value of the SRP index is greater than 1, which implies a wave train with a large amplitude. Note that if two peaks of the SRP index were detected within 10 days, the SRP case with a smaller SRP index was excluded so that the periods of the two cases would not overlap in the lag composite analysis. The central day of the SRP case with the largest absolute value of the SRP index was defined as "day 0" in the lag composite analysis. The SRP cases where PC1 is positive and PC2 is negative are referred to as SRP1+ and SRP2–, respectively.

For the extracted SRP cases, the WB index was defined as the difference in the area-averaged potential temperature at the dynamical tropopause defined by 2 potential vorticity units (PVUs) in the two regions of [30–45°N, 130–160°E] (red box in Fig. 1) and [15–30°N, 130–160°E] (red dashed box in Fig. 1) to investigate whether RWB occurred near Japan. When the WB index is positive, a RWB with a reversal of the meridional gradient of the potential temperature (Pelly and Hoskins 2003) occurs near the Asian jet exit. Hereafter, SRP1+ (SRP2–) cases with WB index greater than 0 (i.e., blocked flow) and less than 0 (i.e., zonal flow) are classified as WB/SRP1+ (WB/SRP2–) cases and ZN/SRP1+ (ZN/SRP2–) cases, respectively. Here, “WB” and “ZN” stand for “wave breaking” and “zonal”, respectively. Since the longitude range defining the WB index is from near Japan to its east, the WB index is expected to more accurately capture the presence or absence of wave breaking in the SRP2– case than that in the SRP1+ case. The longitude range of the WB index (130–160°E) was defined in accordance with Takemura et al. (2020), who showed that the occurrence frequency of RWB peaks in that longitude range. Here, the PJ index is defined as the difference between 850-hPa vorticity anomalies averaged over the [20°–30°N, 110°–140°E] (dashed black box in Fig. 1) and [30°–40°N, 120°–150°E] (solid black box in Fig. 1) regions. Thus, a positive PJ index means the formation of a positive PJ pattern. Results based on the WB and PJ indices are almost the same even if the definition regions of these indices are slightly altered (not shown).

To examine the diffluence and deceleration of the basic flow near the exit of the Asian jet, which is a precondition for RWB (Colucci 2001), the stretching deformation of the basic state (d_B) was derived from the horizontal wind according to Mak and Cai (1989) and Bluestein (1992) as follows:

$$d_B \equiv \frac{\partial u_B}{\partial x} - \frac{\partial v_B}{\partial y}. \quad (2)$$

Here, the subscript *B* denotes the basic state defined by zonal wavenumbers $k < 3$ to exclude the flow associated with Rossby waves. The diffluent and decelerated basic flow thus corresponds to a negative d_B, and is generally found near or upstream of the RWB (e.g., Colucci 2001), contributing to RWB generation.

3. Lag composite analysis of the SRP cases

In this section, we represent the results of lag composite analysis for the four SRP categories based on SRP and RWB defined in section 2 to examine the atmospheric circulation anomalies associated with SRP. Figures 3a and 3b show the central day (day 0) of the SRP1+ and SRP2– cases, respectively. The cases of 73 SRP1+ (red circles in Fig. 3a) and 90 SRP2– (blue circles in Fig. 3b) were extracted if the absolute value of the SRP index was greater than 1 (see section 2). Note that there were many SRP1+ cases from the mid-1970s to the late 1990s, while there were many SRP2– cases after the late 1990s. Such interdecadal variabilities are beyond the scope of this study but have been already reported by Wang et al. (2017) and Liu et al. (2020), who showed two regime shifts of the SRP in the above-mentioned periods, affecting the summer climate over East Asia.

Figure 4a shows a scatter plot of the SRP index on day 0 and the WB index on day +2 for the extracted SRP1+ and SRP2– cases. Numbers of the WB/SRP1+, ZN/SRP1+, WB/SRP2–, and ZN/SRP2– cases are counted in Table 1. Each type of the SRP cases has dozens of events sufficient to perform a composite analysis. To examine a relationship between the RWB and the amplitude of anomalous anticyclone near Japan, a scatter plot of area-averaged anomalous vorticity at 200 hPa near the Asian jet exit and the WB index on day +2 for the SRP cases is shown in Fig. 4b. Here ranges of the area averages are [30°–45°N, 110°–140°E] (red box in Fig. 2a) for the SRP1+ cases and [30°–45°N, 120°–150°E] (red box in Fig. 2b) for the SRP2– cases. The correlation coefficients of 0.44 and 0.49 for SRP1+ and SRP2–, respectively, indicate that the WB index is larger for cases with larger magnitude of anticyclonic anomalies, which is a favorable condition for RWB generation.

3.1. WB/SRP1+ and ZN/SRP1+ cases

Figure 5 shows composite values of 200-hPa and 850-hPa vorticity anomalies, 360-K PV and positive convective precipitation anomalies on days –6, –4, –2, 0, and +2 for the 34 WB/SRP1+ cases. In the upper troposphere, the SRP along the Asian jet gradually amplifies from day –6 to day 0 (Figs. 5a, 5d, 5g, and 5j). Amplification of anticyclonic anomalies associated with the SRP is seen from day –4 to day +2 centered over the area from northeastern China to the Korean peninsula (Figs. 5d, 5g, 5j, and 5m). The zonally elongated anomalous anticyclone associated with the occurrence of RWB is accompanied by the southwestward intrusion of high PV toward immediately north of the Philippines and the consequent enhanced convection near the region (near 20°N, 120°E) during the period (Figs. 5e, 5h, 5k, and 5n). Although the amplitude of SRP attains a maximum on day 0, the occurrence of RWB near Japan is already seen on day –6 and its relationship with the SRP is unclear. In the lower troposphere, the enhanced convective activity during this period results in the formation of a positive PJ pattern with a significant anomalous cyclone to the southwest of Japan and a significant anomalous anticyclone near the mainland Japan (Figs. 5i, 5l, and 5o). The above features are a typical example of how SRP excites a positive PJ pattern through RWBs, consistent with Takemura and Mukougawa (2020a). Enhanced convection and a positive PJ-like pattern are already seen on day –4, which is associated with the amplifying SRP and the related occurrence of RWB. The amplitude of the SRP on day 0 (Fig. 5j) near East Asia is smaller than that over Eurasia but much larger than that of the regressed upper-level vorticity anomaly in Fig. 2a. This feature implies that the excited PJ pattern recursively intensifies the SRP near East Asia through a feedback process between them.

On the other hand, the composited anomalies of 39 ZN/SRP1+ case are shown in Fig. 6. In the upper troposphere, as in the case of WB/SRP1+, the SRP along the Asian jet gradually amplifies from day –4 to day 0 (Figs. 6d, 6g, and 6j). However, the upper-level anomalous anticyclone over northeastern China is weaker than the WB/SRP1+ case (Fig. 5j). The lack of development of an anticyclone, which does not have a zonally-elongated shape as in the case of WB/SRP1+, is consistent with the lack of RWB in the region and scattered convection to the south of Japan from day –2 to day +2 (Figs. 6h, 6k, and 6n). The SRP extends further downstream from the anomalous anticyclone we are now focusing on to the North Pacific region east of Japan from day 0 to day +2 (Figs. 6j and 6m), also indicating the absence of RWB. In the lower troposphere, unlike the WB/SRP1+ case, there are no meridional dipole anomalies corresponding to the positive PJ pattern from day –2 to day +2 (Figs. 6i, 6l, and 6o). This result indicates that SRPs without RWBs are less likely to excite positive PJ patterns than SRPs with RWBs, indicating that RWBs play a crucial role in the formation of PJ patterns.

To compare the horizontal structure of the Asian jet with and without RWB, the difference in d_B on day 0 between the WB/SRP1+ case and the ZN/SRP1+ case is shown in Fig. 7a. The stretching deformation of the WB/SRP1+ case is significantly negative, and its magnitude is larger than the ZN/SRP1+ case in the vicinity and west of the region where RWBs occur, indicating favorable conditions for RWB generation in the WB/SRP1+ case.

3.2. WB/SRP2– and ZN/SRP2– cases

Figure 8 shows the composite anomalies for the 37 WB/SRP2– cases. In the upper troposphere, amplification of the SRP along the Asian jet and anticyclonic anomaly around Japan associated with the RWB are seen from day –4 to day 0 (Figs. 8d, 8g, and 8j). Although the anomalous anticyclone is already seen over northern China on day –6 (Fig. 8a), its amplification with the slight eastward migration over the Sea of Japan is closely associated with the SRP amplification (Figs. 8d, 8g, and 8j). The amplified anticyclone is associated with the RWB, inducing southwestward intrusion of high PV toward southeast of Japan and resulting in the enhancement of convection south of Japan (near 25°N, 130°E) from day –2 to day +2 (Figs. 8h, 8k, and 8n). During this period, the enhanced convection south of Japan promotes the formation of positive PJ patterns (Figs. 8i, 8l, and 8o). This result indicates that the SRP of the WB/SRP2– case can excite the positive PJ pattern as the WB/SRP1+ case through the RWB. Although enhanced convection and a positive PJ-like pattern are already seen from day –6 to day –4 as in the WB/SRP1+ cases, the anomalous convection is scattered. Afterwards, the enhanced convection gradually become organized in association with the RWB. As in the WB/SRP1+ cases, the amplitude of the SRP on day 0 (Fig. 8m) is enhanced near East Asia, suggesting that the excited PJ pattern recursively intensifies the SRP near East Asia through a feedback process between them.

On the other hand, Figure 9 shows the composite anomalies for the 53 ZN/SRP2– cases. Although SRP amplification is clearly seen along the Asian jet in the upper troposphere from day –4 to day 0 (Figs. 9d, 9g, and 9j), the upper-level anomalous anticyclone near Japan is weaker than in the WB/SRP2– case. The lack of a well-developed anticyclone is consistent with the absence of a RWB in the region and scattered convection to the southeast of Japan from day –2 to day +2 (Figs. 9h, 9k, and 9n). The SRP extends further downstream from the anomalous anticyclone we are now focusing on to the North Pacific region east of Japan from day 0 to day +2 (Figs. 9j and 9m), which indicates that there is still no RWB. In the lower troposphere, the positive PJ pattern is not excited during the period (Figs. 9i, 9l, and 9o). The composite analysis of the two cases also shows that RWBs play a crucial role in the formation of positive PJ patterns.

The difference in d_B on day 0 between the WB/SRP2– and ZN/SRP2– cases is shown in Fig. 7b. Near Japan, the stretching deformation of the WB/SRP2– case is significantly negative, and its magnitude is larger than that of the ZN/SRP2– case, indicating favorable conditions for RWB generation in the WB/SRP2– case.

4. Estimated ratio of positive PJ pattern

In this section, we estimate the percentage of SRPs in which positive PJ patterns occur in order to examine the probability of PJ pattern occurrence for the four types of SRPs described above. Figure 10 shows a scatter plot of the SRP index on day 0 and the WB index on day +2 for all extracted SRP cases, with blue circles indicating cases with a positive PJ index on day +2. Positive PJ patterns are more common in the case of SRPs with RWBs (WB/SRP1+ and WB/SRP2–) than in the case of SRPs without RWBs (ZN/SRP1+ and ZN/SRP2–). In the WB/SRP1+ and WB/SRP2– cases, SST anomalies near the subtropical WNP are not significant (not shown), indicating negligible contribution to promoting positive PJ patterns, consistent with Takemura and Mukougawa (2020a). The SST anomalies, by contrast, clearly show a La Niña-like pattern in the equatorial Pacific (not shown), suggesting favorable conditions for RWB occurrence through modulated tropical convection and a northward-shifted Asian jet, which was indicated by Takemura et al. (2020). The figure on the right side of the scatter plot in Fig. 10 is a histogram of the WB index, which is further classified into cases where the PJ index is positive and the other cases. For most of the SRPs, the WB index tends to shift positively when there is a PJ pattern and negatively when there is not. The difference in the mean value of WB indices between SRPs with and without positive PJ pattern is statistically significant at the 99% confidence level.

Table 2 shows the number and ratio of cases with and without positive PJ patterns for the four SRP cases. In SRP cases where RWBs are present, i.e., WB/SRP2– and WB/SRP1+ cases, about 70% and 60%, respectively, are accompanied by positive PJ patterns. On the other hand, about half of the SRP cases without RWB (i.e., ZN/SRP2– and ZN/SRP1+ cases) are accompanied by positive PJ patterns. This change in the ratio of positive PJ patterns with and without RWB suggests that RWB plays a role in increasing the probability of causing positive PJ patterns. The percentage of WB/SRP2– cases with positive PJ patterns is about 70%, which is larger than the percentage of WB/SRP1+ cases with positive PJ patterns (about 60%). Because the PJ pattern emerges climatologically from near Japan to its south (Nitta 1987, Kosaka and Nakamura 2010), RWBs near Japan (i.e., WB/SRP2–) are more likely to induce a positive PJ pattern than RWBs to the west of Japan (i.e., WB/SRP1+) from a geographical perspective. The percentage of positive PJ patterns triggered by the SRP is not outstandingly high, but not negligibly small. This supports an important role of the SRP accompanied by the RWB near Japan in triggering positive PJ patterns.

The other SRPs are cases that do not invoke a positive PJ pattern (i.e., open circles in WB/SRP1+ and WB/SRP2– in Fig. 10) and are referred to as exceptional cases in the following. As mentioned in section 1, Takemura and Mukougawa (2022) showed that PJ patterns without RWB are closely related to tropical SST anomalies and the summertime bi-week and intraseasonal oscillations (i.e., BSISO) of tropical convection. Their results imply that exceptional cases are strongly influenced by tropical SST and convective activity anomalies, indicating a “pure” influence of the tropics. The results of an additional composite analysis of tropical SST and convective precipitation for the exceptional case show the same characteristics as those of Takemura and Mukougawa (2022) (not shown). Our results suggest that the PJ pattern is mainly influenced by tropical SST anomalies and the corresponding convective activity, but also can be excited by the characteristic mid-latitude atmospheric circulation anomalies, namely SRP with RWB. Note that the excited PJ pattern also has a possibility to intensify the magnitude of the SRP near East Asia, as described in Sections 3.1 and 3.2. This possible feedback process between the SRP and PJ patterns is supported by Lu and Lin (2009), who indicated that precipitation anomalies over the subtropical WNP can significantly affect large-scale circulations and may be crucial for the maintenance of the meridional teleconnection over the WNP and East Asia during summer. Further studies should carefully evaluate the contribution of the SRP to PJ patterns with RWBs in more detail.

5. Conclusions and discussions

This study examined the ratio of SRP cases triggering the formation of positive PJ patterns through RWBs near the Asian jet exit region. The SRP cases were detected using the first two PCs of meridional winds in the upper troposphere over Eurasia and characterized by the presence of an the upper-level anticyclonic over the Yellow Sea or Japan. They were further classified into those with and without RWBs. In the case of SRP with RWB, the anticyclonic circulation anomaly near the Asian jet exit has a more zonally extended shape and larger amplitude than in the case without RWB.

Composite analysis of the SRP with RWB showed that high PV intrudes southwestward toward the south of the RWB, excites enhanced convection in this region, and results in the formation of a positive PJ pattern. In contrast, composite anomalies in the case of the SRP without RWB, although wave trains exist over a wide area from Eurasia to Japan, convection is not enhanced south of Japan and no positive PJ pattern is formed. Estimation using the scatter plots of SRP, WB, and PJ indices (Fig. 10) showed that the percentage of the formation of positive PJ patterns in SRP cases with RWBs is approximately 60–70%, while approximately 40–50% in SRP cases without RWBs, confirming that the presence of RWBs increases the percentage of the formation of positive PJ patterns by a factor of 1.2 to 1.7. There were two exceptional cases of SRP: one with no RWB and a positive PJ pattern, and the other with RWB but no positive PJ pattern are strongly affected by tropical SST anomalies and convective activity, consistent with Takemura and Mukougawa (2022).

The relationship between the SRP and PJ pattern has been shown to be reproducible in climate model simulations (e.g., Gong et al. 2018), suggesting predictability of the dynamical relationship. Takemura et al. (2021) showed from sensitivity analysis of ensemble forecasts that the predictability of a PJ pattern event is closely associated with RWB to the east of Japan as well as SRP. Takemura and Mukougawa (2021a) further indicated from nudging experiments using an atmospheric general circulation model that better prediction of SRP with RWB can improve the reproducibility of PJ patterns. Evaluating the reproduced relationship between the SRP and PJ pattern provides a better understanding of the dynamical relationship between them.

Our results show that RWBs near Japan play an important role in triggering positive PJ patterns, and that SRP with RWBs increases the probability with which positive PJ patterns are excited, supporting the results of Takemura and Mukougawa (2020a). The result on the classification of positive PJ events conducted by Takemura and Mukougawa (2022) indicated that the positive PJ events accompanied by RWB account for approximately 20% of the whole positive PJ events. We have to address the question of how much of RWB seen in the positive PJ events is explained by SRP and the causality between them for the next study.

Data Availability Statement

The datasets analyzed in this study (the Japanese 55-year reanalysis; JRA-55) including an element of convective precipitation are available at https://jra.kishou.go.jp/JRA-55/index_en.html.

Acknowledgments

The Generic Mapping Tools (GMT) were used for the graphics. This study was partly supported by the JSPS KAKENHI Grant (18H01280).

References

Abatzoglou, J. T., and G. Magnusdottir, 2006: Planetary wave breaking and nonlinear reflection: Seasonal cycle and interannual variability. J. Climate, 19, 6139–6152.

Bluestein, H. B., 1992: Synoptic-Dynamic Meteorology in Midlatitudes. Vol. 1. Oxford University Press, 431 pp.

Chiang, J. C. H., and D. J. Vimont, 2004: Analogous Pacific and Atlantic meridional modes of tropical atmosphere-ocean variability, *J. Climate*, **17**, 4143–4158.

Colucci, S. J., 2001: Planetary-scale preconditioning for the onset of blocking. *J. Atmos. Sci.*, **58**, 933–942.

Duchon, C. E, 1979: Lanczos filtering in one and two dimensions. *J. Appl. Meteor.*, **18**, 1016–1022.

Enomoto, T., B. J. Hoskins, and Y. Matsuda, 2003: The formation mechanism of the Bonin high in August. *Quart. J. Roy. Meteor. Soc.*, **129**, 157–178.

Enomoto, T., 2004: Interannual variability of the Bonin high associated with the propagation of Rossby waves along the Asian jet. *J. Meteor. Soc. Japan*, **82**, 1019–1034.

Enomoto, T., H. Endo, Y. Harada, W. Ohfuchi, 2009: Relationship between high-impact weather events in Japan and propagation of Rossby waves along the Asian jet in July 2004. *J. Meteor. Soc. Japan*, **87**, 139–156.

Gong, H., L. Wang, W. Chen, R. Wu, G. Huang, and D. Nath, 2018: Diversity of the Pacific–Japan pattern among CMIP5 models: Role of SST anomalies and atmospheric mean flow, *J. Climate*, **31**, 6857-6877.

Hong, X., R. Lu, and S. Li, 2018: Asymmetric relationship between the meridional displacement of the Asian westerly jet and the Silk Road pattern, *Adv. Atmos. Sci.*, **35**, 389–396.

Kikuchi, K., B. Wang, and Y. Kajikawa, 2012: Bimodal representation of the tropical intraseasonal oscillation. *Climate Dyn.*, **38**, 1989–2000.

Kikuchi, K., 2021: The boreal summer intraseasonal oscillation (BSISO): A review. *J. Meteor. Soc. Japan*, **99**, 933–972.

Kobayashi, S., Y. Ota, Y. Harada, A. Ebita, M. Moriya, H. Onoda, K. Onogi, H. Kamahori, C. Kobayashi, H. Endo, K. Miyaoka, and K. Takahashi, 2015: The JRA-55 reanalysis: General specifications and basic characteristics. *J. Meteor. Soc. Japan*, **93**, 5−48.

Kosaka, Y., and H. Nakamura, 2006: Structure and dynamics of the summertime Pacific-

Japan teleconnection pattern. *Quart. J. R. Met. Soc.*, **132**, 2009-2030.

Kosaka, Y., H. Nakamura, M. Watanabe, and M. Kimoto, 2009: Analysis on the dynamics of a wavelike teleconnection pattern along the summertime Asian Jet based on a reanalysis dataset and climate model simulations. J. Meteor. Soc. Japan, 87, 561–580.

Kosaka, Y., and H. Nakamura, 2010: Mechanisms of meridional teleconnection observed between a summer monsoon system and a subtropical anticyclone. Part I: The Pacific-Japan pattern. J. Climate, 23, 5085–5108.

Lee, J. T., B. Wang, M. C. Wheeler, X. Fu, D. E. Waliser, and I.-S. Kang, 2013: Real-time multivariate indices for the boreal summer intraseasonal oscillation over the Asian summer monsoon region. *Climate Dyn.*, **40**, 493–509.

Liu, Y., W. Zhou, X. Qu, and R. Wu, 2020: An interdecadal change of the boreal summer Silk Road pattern around the late 1990s, *J. Climate*, **33**, 7083–7100.

Lu, R., and B. W. Dong, 2001: Westward extension of North Pacific subtropical high in summer. *J. Meteor. Soc. Japan*, **79**, 1229–1241.

Lu, R.-Y., J.-H. Oh, and B.-J. Kim, 2002: A teleconnection pattern in upper-level meridional wind over the North African and Eurasian continent in summer, *Tellus*, **54**, 44–55.

Mak, M., and M. Cai, 1989: Local barotropic instability. J. Atmos. Sci., 46, 3289–3311.

Nitta, T., 1987: Convective activities in the tropical western Pacific and their impact on the Northern Hemisphere summer circulation. *J. Meteor. Soc. Japan*, **65**, 373–390.

Pelly, J. L., and B. J. Hoskins, 2003: A new perspective on blocking. *J. Atmos. Sci.*, **60**, 743–

755.

Postel, G. A., and M. H. Hitchman, 1999: A climatology of Rossby wave breaking along the subtropical tropopause. J. Atmos. Sci., 56, 359–373.

Postel, G. A., and M. H. Hitchman, 2001: Observational diagnosis of a Rossby wave breaking event along the subtropical tropopause. Mon. Wea. Rev., 129, 2555–2569.

Seiki, A., Y. Kosaka, and S. Yokoi, 2021: Relationship between the boreal summer intraseasonal oscillation and the Pacific-Japan pattern and its interannual modulations. *SOLA*, **17**, 177–183.

Song, F., T. Zhou, and L. Wang, 2013: Two modes of the Silk Road pattern and their interannual variability simulated by LASG/IAP AGCM SAMIL2.0, *Adv. Atmos. Sci.*, **30**, 908–921.

Takaya, K., and H. Nakamura, 2001: A formulation of a phase-independent wave-activity flux for stationary and migratory quasigeostrophic eddies on a zonally varying basic flow. *J. Atmos. Sci.*, **58**, 608–627.

Takaya, Y., 2019: Positive phase of Pacific meridional mode enhanced western North Pacific tropical cyclone activity in summer 2018. *SOLA*, **15A**, 55–59.

Takemura, K., Y. Kubo, and S. Maeda, 2017: Relation between a Rossby wave-breaking event and enhanced convective activities in August 2016. SOLA, 13, 120–124.

Takemura, K. and H. Mukougawa, 2020a: Dynamical Relationship between Quasi-stationary Rossby Wave Propagation along the Asian Jet and Pacific-Japan Pattern in Boreal

Summer, *J. Meteor. Soc. Japan*, **98**, 169–187.

Takemura, K. and H. Mukougawa, 2020b: Maintenance Mechanism of Rossby Wave Breaking and Pacific-Japan Pattern in Boreal Summer, *J. Meteor. Soc. Japan*, **98**, 1183–1206.

Takemura, K., H. Mukougawa, and S. Maeda, 2020: Large-scale atmospheric circulation related to frequent Rossby wave breaking near Japan in boreal summer, *J. Climate*, **33**, 6731–6744.

Takemura, K., H. Mukougawa, and S. Maeda, 2021: Interdecadal Variability of Rossby Wave Breaking Frequency near Japan in August, *SOLA*, **17**, 125–129.

Takemura, K., T. Enomoto, and H. Mukougawa, 2021: Predictability of enhanced monsoon trough related to the meandered Asian jet and consequent Rossby wave breaking in late August 2016, *J. Meteor. Soc. Japan*, **99**, 339–356.

Takemura, K., and H. Mukougawa, 2021a: Relaxation experiments for predictability assessment of enhanced monsoon trough in late August 2016, *J. Meteor. Soc. Japan*, **99**, 459–472.

Takemura, K. and H. Mukougawa, 2021b: Tropical cyclogenesis triggered by Rossby wave breaking over the western North Pacific, *SOLA*, **17**, 164–169.

Takemura, K. and H. Mukougawa, 2022: A new perspective of Pacific–Japan pattern: Estimated percentage of the cases triggered by Rossby wave breaking, *J. Meteor. Soc. Japan*, Early Online Released.

Wakabayashi, S., and R. Kawamura, 2004: Extraction of major teleconnection patterns possibly associated with anomalous summer climate in Japan. *J. Meteor. Soc. Japan*, **82**, 1577–1588.

Wang, L., P. Xu, W. Chen, and Y. Liu, 2017: Interdecadal variations of the Silk Road pattern. J. Climate, 30, 9915–9932.

Xie, S.-P., K. Hu, and J. Hafner, 2009: Indian Ocean capacitor effect on Indo-Western pacific climate during the summer following El Niño. *J. Climate*, **22**, 730–747.

Xie, S.-P., Y. Kosaka, Y. Du, K. Hu, J. S. Chowdary, and G. Huang, 2016: Indo-western Pacific ocean capacitor and coherent climate anomalies in post-ENSO summer: A review. *Adv. Atmos. Sci.*, **33**, 411–432.

Zhou, F., R. Zhang, J. Han, 2019: Relationship between the circumglobal teleconnection and Silk Road pattern over Eurasian continent, *Science Bulletin*, **64**, 374–376.

Zhu, Y., Z. Wen, Y. Guo, R. Chen, X. Li, and Y. Qiao, 2020: The characteristics and possible growth mechanisms of the quasi-biweekly Pacific–Japan teleconnection in Boreal Summer. *Clim. Dyn.*, **55**, 3363–3380.

List of Figures

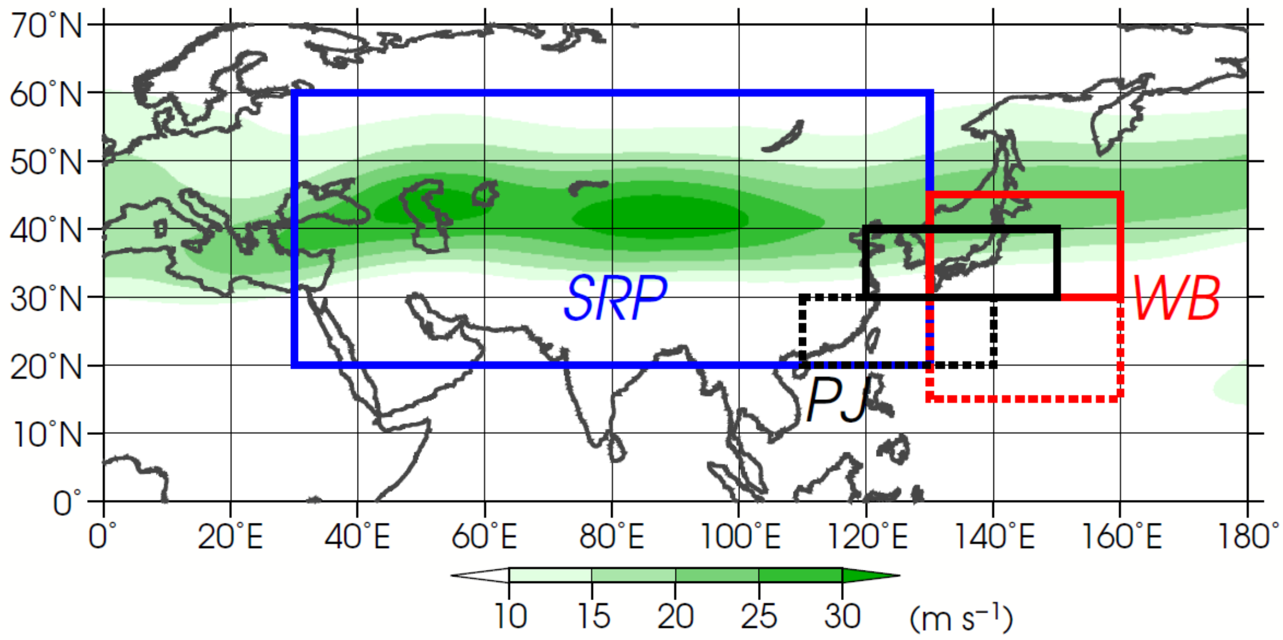

Fig. 1 The area where EOF analysis of 200-hPa meridional wind anomalies for July–August is performed to define the SRP index (blue box), and the areas where area averages are calculated to define the WB index (red solid and dashed boxes) and the PJ index (black solid and dashed boxes). See text for detailed definitions. Green shading indicates climatological zonal wind at 200 hPa in July–August (unit: m s^{-1}).

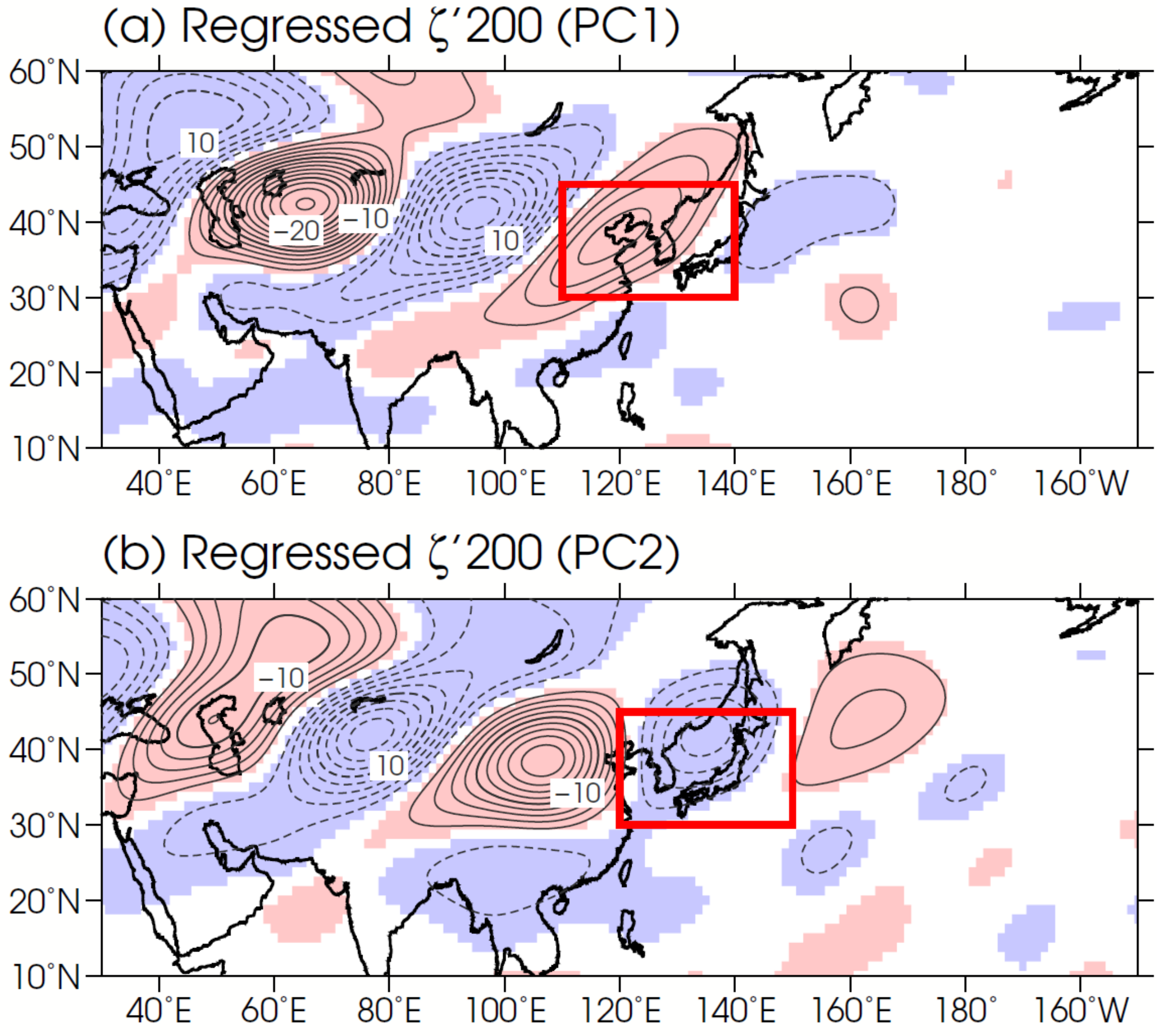

Fig. 2 200-hPa vorticity anomalies (contours) regressed on (a) PC1 and (b) PC2 scores of monthly mean 200-hPa meridional wind anomalies in the region of [20–60^{o}N, 30–130^{o}E] (blue box in Fig. 1) during July and August. The dashed and solid contours indicate positive and negative vorticity anomalies, respectively, with the interval of 2×10^{-6} s^{-1}. Cold- and warm-colored shadings indicate regressions of cyclonic and anticyclonic anomalies that are significant at the 99.9% confidence level, respectively.

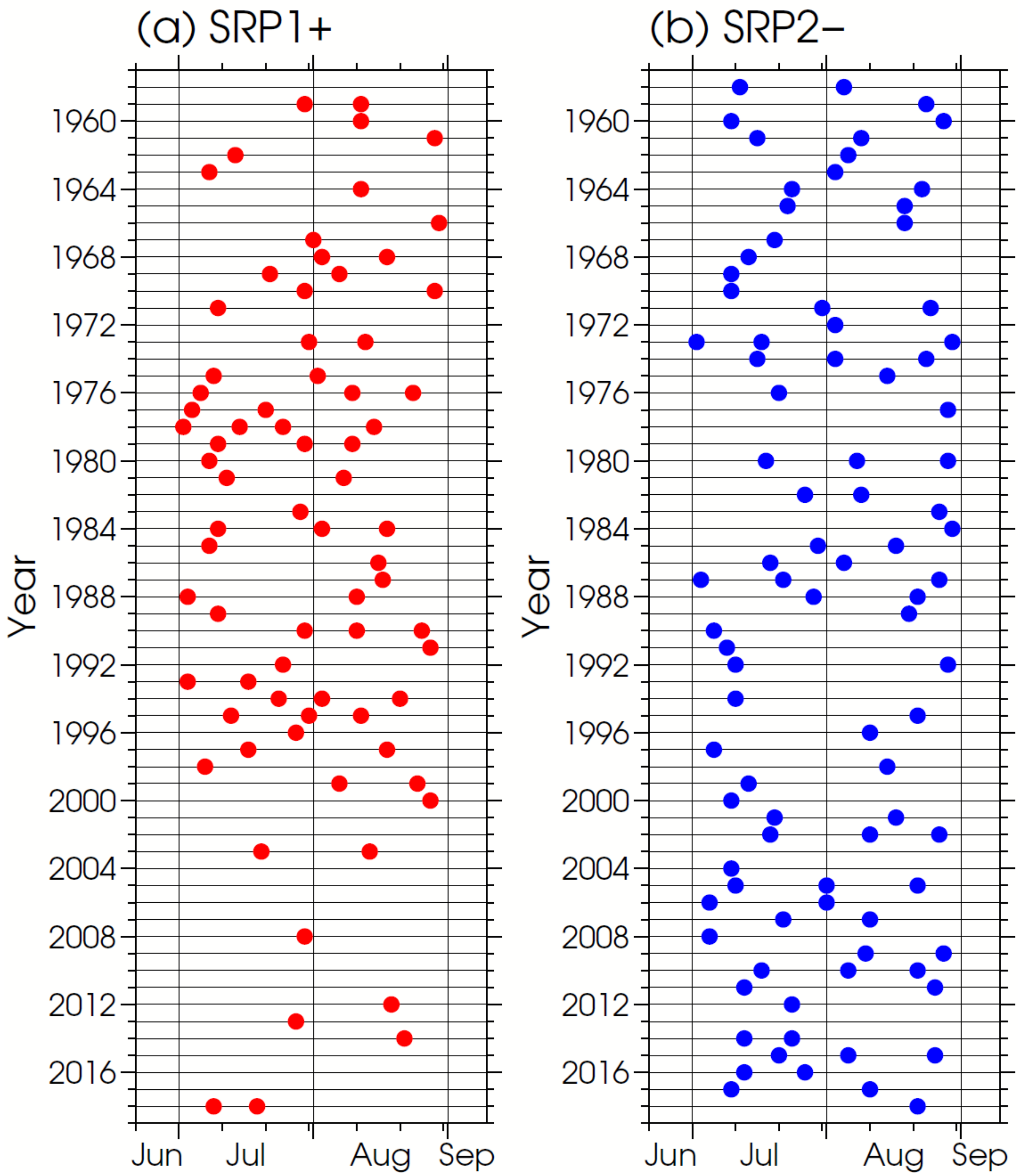

Fig. 3 Center date (day 0) of the extracted SRP1+ (red circles) and SRP2– (blue circles) cases. Thin vertical lines represent the first day of each month.

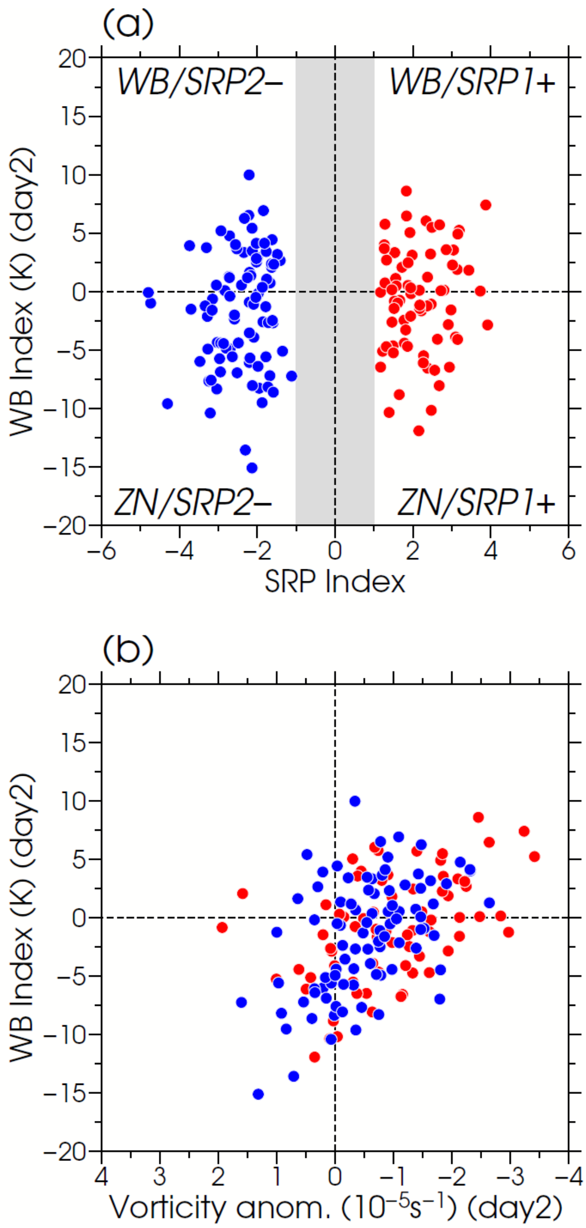

Fig. 4 (a) Scatter plot of SRP index on day 0 and WB index on day +2 (unit: K) for the cases of SRP1+ (red circles) and SRP2– (blue circles). Gray shading indicates the range of SRP index from –1 to +1. (b) Scatter plot of area-averaged 200-hPa vorticity anomalies around Japan and WB index on day +2 in the SRP case. The range of the area averages is [30°–45°N, 110°–140°E] for SRP1+ (red circles) and [30°–45°N, 120°–150°E] for SRP2– (blue circles).

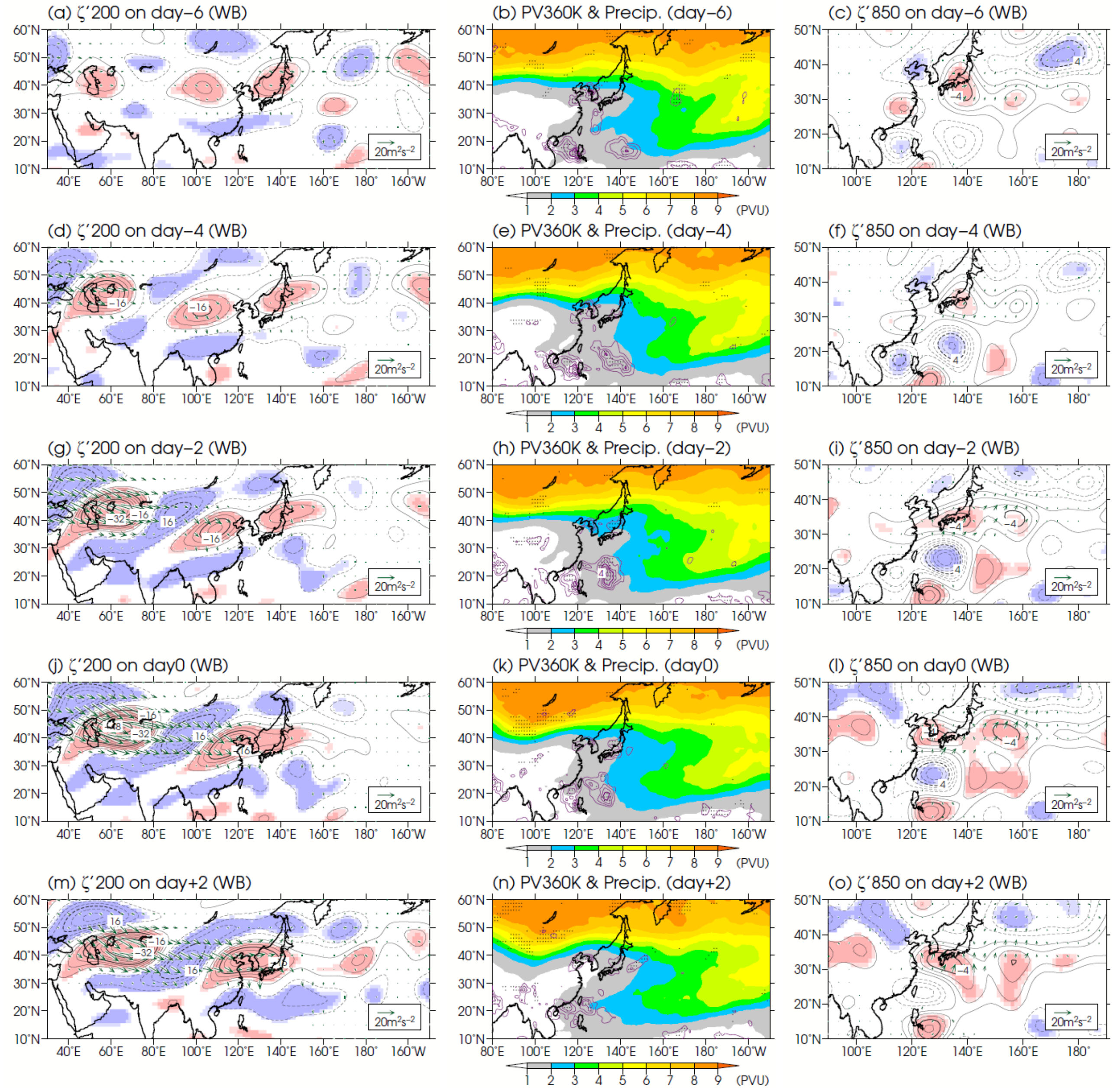

Fig. 5 Composite of 5-day running mean (left) 200-hPa vorticity anomalies (contours, unit: 10^{-6} s^{-1}), (middle) 360-K potential vorticity (shading, unit: PVU) and positive convective precipitation (contour interval: 1 mm d^{-1}), and (right) 850-hPa vorticity anomalies (contours) for the WB/SRP1+ case. The solid and dashed contours represent negative and positive vorticity anomalies, respectively. The green vectors indicate WAF (unit: m^{2} s^{-2}). The light (dark) shading in the left and right panels and the dots in the center panel

indicate that the vorticity and positive convective precipitation anomalies are significant at the 90% (95%) confidence level, respectively. (a, b, c) day –6, (d, e, f) day –4, (g, h, i) day –2, (j, k, l) day 0, and (m, n, o) day +2.

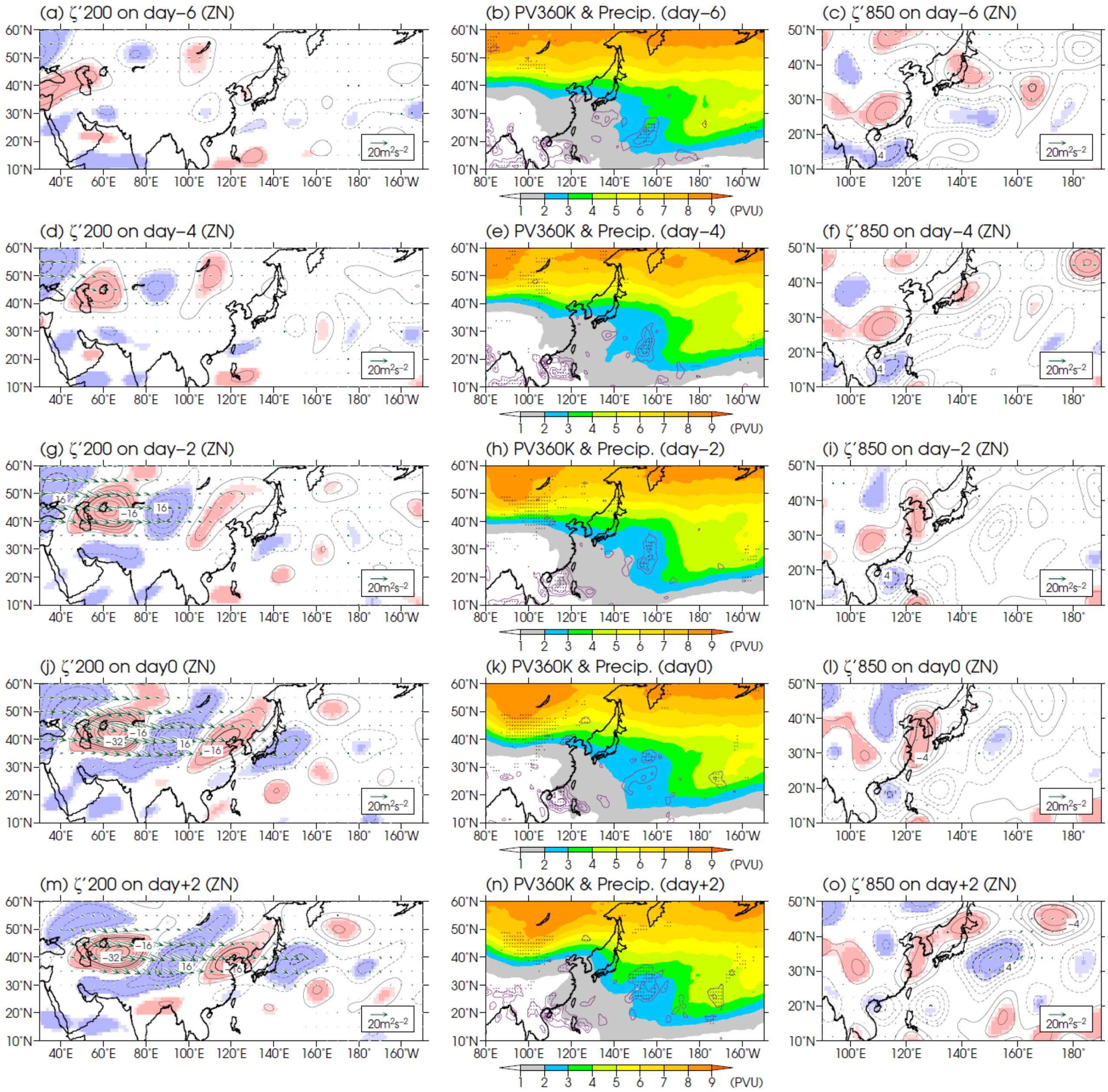

Fig. 6 Same as Fig. 5, but for the ZN/SRP1+ case.

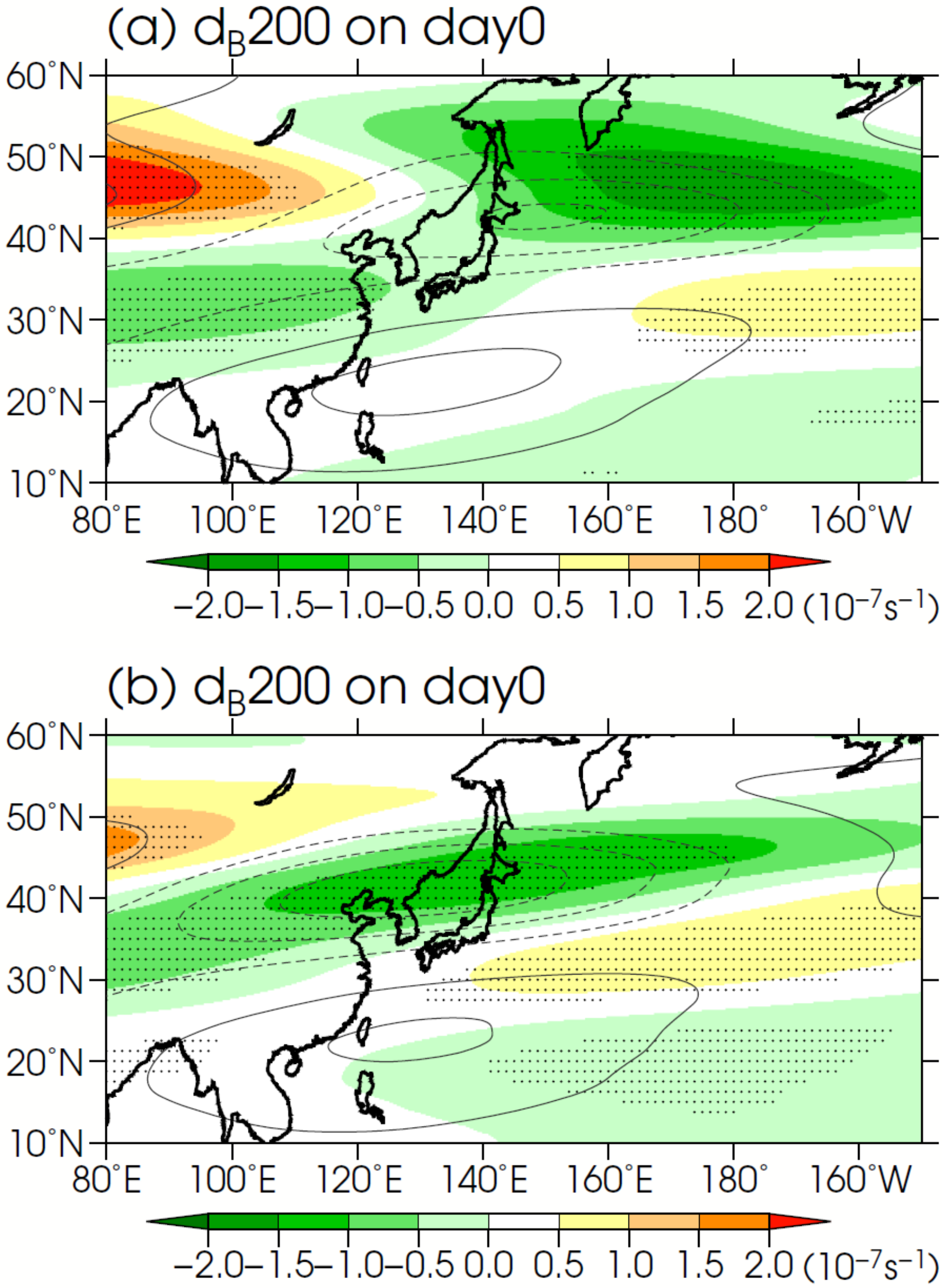

Fig. 7 (a) Difference in stretching deformation (d_B) at 200 hPa between the WB/SRP1+ and ZN/SRP1+ cases on day 0 (shading, unit: 10^{-7} s^{-1}). The contours show the stretching deformation of the WB/SRP1+ cases. Dots indicate regions where the difference in the stretching deformation is significant at the 95% confidence level. (b) Same as (a), but for the WB/SRP2– and ZN/SRP2– cases.

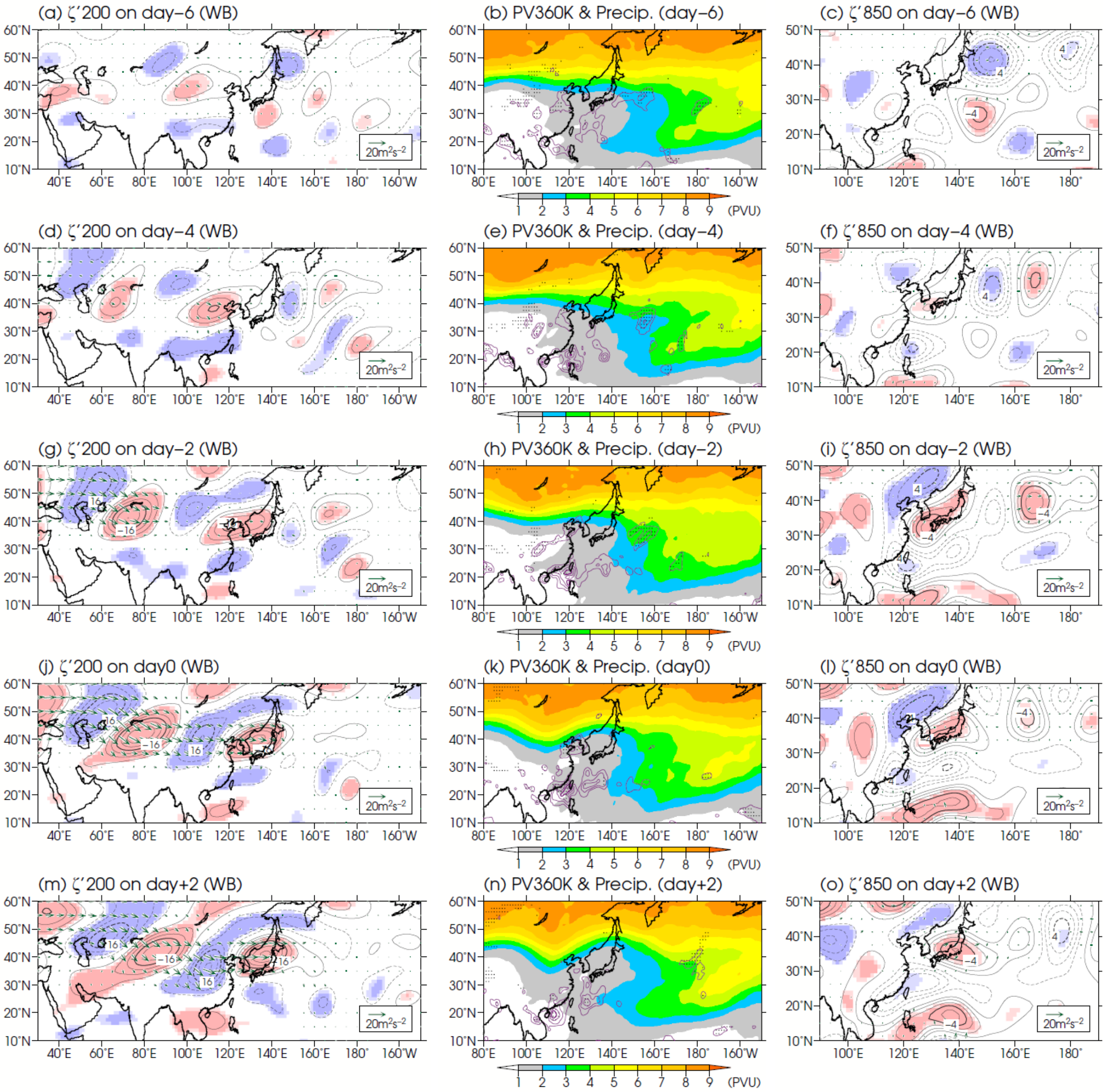

Fig. 8 Same as Fig. 5, but for the WB/SRP2– case.

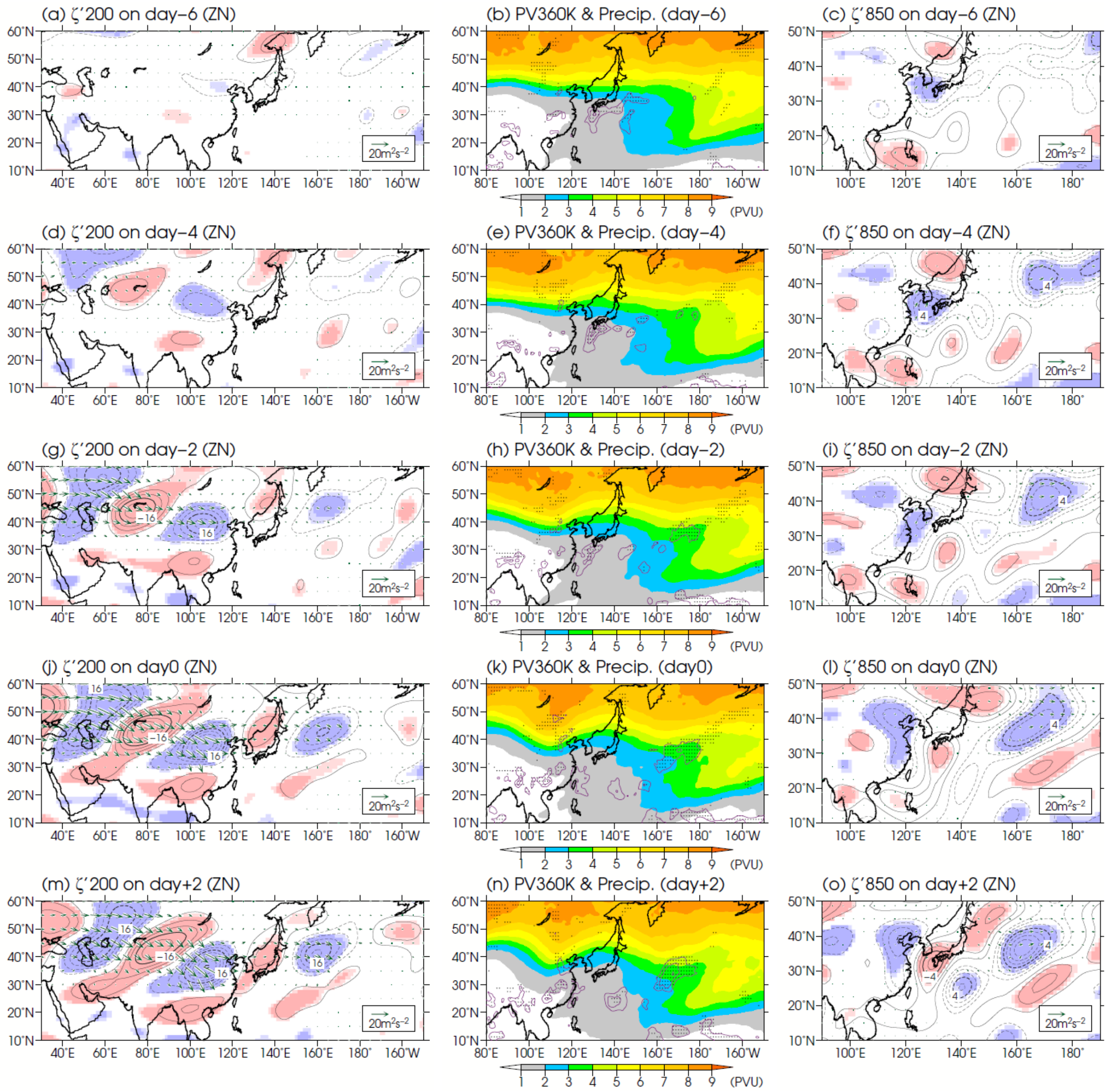

Fig. 9 Same as Fig. 5, but for the ZN/SRP2– case.

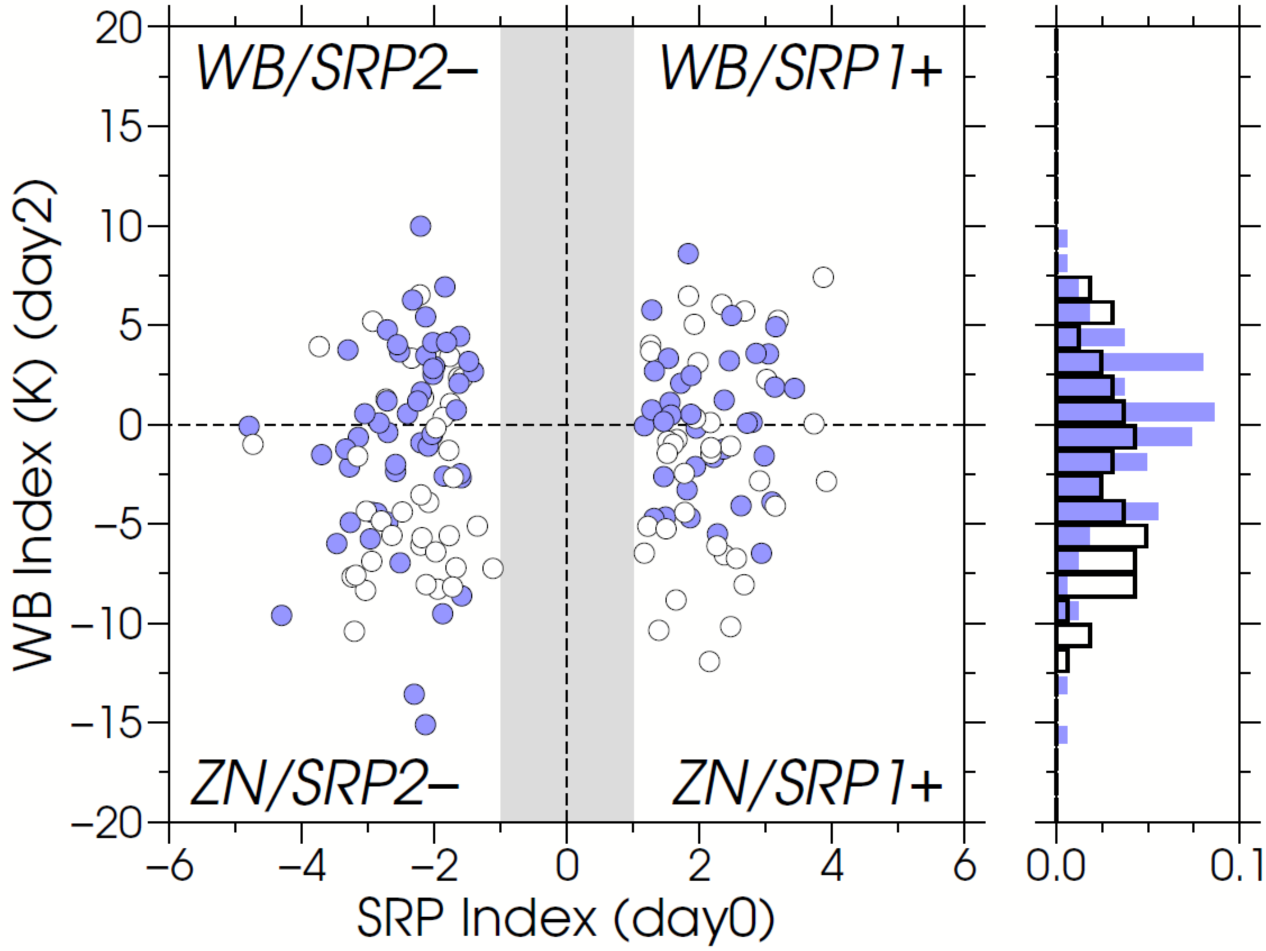

Fig. 10 Same as Fig. 4a, but for the blue and white circles indicate positive and negative PJ indices on day +2, respectively. The right figure shows the histogram of WB index for the SRP case with (blue bars) and without (white bars) a positive PJ pattern, where the frequency distribution is normalized by the number of samples and the bin width is 1.25K.

List of Tables

Table 1 Number of SRP cases of the four types classified into the cases with RWB (WB/SRP1+, WB/SRP2–) and without RWB (ZN/SRP1+, ZN/SRP2–).

	SRP2–	SRP1+
WB	37	34
ZN	53	39

Table 2 Number and percentage (unit: %) of four types of SRP cases (WB/SRP1+, WB/SRP2–, ZN/SRP1+, and ZN/SRP2–) classified by the presence (labeled by “PJ”) or absence (labeled by “noPJ”) of a positive PJ pattern using the PJ index on day +2. The percentages are calculated separately for the four different types of SRP.

SRP2–		SRP1+	
WB/PJ	WB/noPJ	WB/PJ	WB/noPJ
25 (68%)	12 (32%)	21 (62%)	13 (38%)
ZN/noPJ	ZN/PJ	ZN/noPJ	ZN/PJ
26 (49%)	27 (51%)	23 (59%)	16 (41%)